Convergence test for inversion of frequency-resolved optical gating spectrograms

Daniel J. Kane

Southwest Sciences, Inc., Suite E-11, 1570 Pacheco Street, Santa Fe, New Mexico 87505

Fiorenzo G. Omenetto and Antoinette J. Taylor

Los Alamos National Laboratories, Los Alamos, New Mexico 87545

Received April 28, 2000

We describe a new and simple method to aid in the analysis of retrieved pulses from inverted frequency-resolved optical gating (FROG) traces. The analysis can separate noise from distortion and shows that distortion is more deleterious to the retrieved pulse than is pure noise. The analysis relies on the fact that FROG traces can be constructed from a single outer product of two vectors, whereas distortion and noise require the sum of a series of outer products. © 2000 Optical Society of America

OCIS codes: 100.3190, 100.5070, 320.5550, 320.7100.

Intensity and phase measurement of ultrashort laser pulses has become more important. One well-known pulse-measurement technique is frequency-resolved optical gating[1–5] (FROG), in which a spectrogram of a pulse is constructed optically by interaction of a gate pulse in a nonlinear optical medium with the pulse to be measured. The interaction forms a signal pulse that is spectrally resolved at a series of time delays. A two-dimensional phase-retrieval algorithm is used to invert a spectrogram of N^2 points to yield a complex pulse of length N.

The two-dimensional phase-retrieval algorithm is iterative, converging to a pulse that minimizes the difference between the measured and the calculated FROG traces (FT's). The inversion algorithm is assumed to be converged when the FT error is small (average rms deviation per pixel, typically 0.1–2%), and the retrieved FT appears similar to the experimental FT.[2] The most common criticisms of FROG have been its inability to determine effectively the convergence of the algorithm or the rate of convergence and its inability to determine the precision of the results.[6] However, unlike direct pulse-measurement techniques,[7] FROG has useful cross checks for evaluating the success (or failure) of the FROG measurement.[2]

In this Letter we add to FROG's cross checks by defining a new convergence criterion and developing a new convergence analysis for FROG, spectrogram, or sonogram inversions[8–10] (Fig. 1). This new convergence criterion, noise-limited convergence, is the best possible convergence for any given spectrogram inversion in the presence of noise. Although the FT error defines how well the retrieved pulse matches the data constraint, our analysis evaluates how well the measured spectrogram matches the mathematical form constraint by systematically decomposing the measured spectrogram into the contributions made by the retrieved pulse, retrieved gate, noise, and distortions. We demonstrate the use of this method on both synthetic and experimental data. Our method is easy to implement and general and can be automated.

Previous work has shown that a FT can be constructed from the outer product of two vectors (Fig. 1), the pulse to be measured and the gate; simple point manipulation transforms the outer product matrix to the time domain of the FT.[3–5] Fourier transforming the columns converts the time domain into the frequency domain. The magnitude squared of the result yields the FT. The reverse is also true: Given a perfect FT, with the proper phase, the original vectors can be obtained by use of a singular value decomposition[11] (SVD) of the outer product form matrix.[3–5]

For a perfect FT a SVD of the outer product form matrix yields only one outer product pair; however, FROG inversion is overdetermined. As a result, a perfect FT (in the strict mathematical sense) can never be measured. The noise that is present in the detection system and distortions caused by geometrical effects, bandwidth limitations, etc. convert FT's into images that can no longer be described by a single outer product pair—a superposition of weighted outer products is required. All inversion algorithms discard the extraneous information provided by the outer products other than the principal vector pair (the vector pair with the largest weight).[3–5] However, the shape of the function

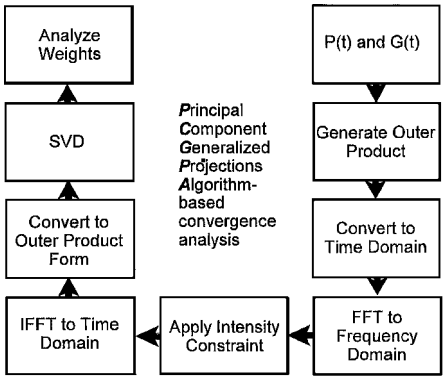

Fig. 1. Steps required for SVD analysis of a FT. IFFT, inverse fast Fourier transform; FFT, fast Fourier transform.

0146-9592/00/161216-03$15.00/0

formed when the weights of these outer products are plotted in decreasing order provides information about the convergence of the algorithms (Fig. 4, below).

To illustrate our method we have produced six synthetic FT's with various amounts of added noise and distortion, which are shown in Fig. 2. FT 1 is perfect and undistorted, with no noise. FT 2 is the same FROG trace but with shot noise added. FT 3 is FT 1 with only additive noise. FT 4 is FT 1 with both shot and additive noise. FT 4 is filtered by removal of the high frequencies in a two-dimensional fast Fourier transform to produce FT's 5 and 6. All the FT's shown in Fig. 2 were inverted with 200 iterations of the second-harmonic-generation principal components generalized projections (SHG-PCGP) algorithm.[4] The time and frequency marginals were calculated from the retrieved pulses from FT's 4–6 and are compared with the marginals for FT 1, as shown in Fig. 3. The agreement is excellent.

Figure 4 shows outer product weight plots for the FT's in Fig. 2. FT 1, the perfect FROG trace, has only one nonzero outer product weight. All the other FT's depicted in Fig. 2 show more than one nonzero outer product weight because added noise and distortions convert the FT's to images. For example, when FT's 2–4, consisting of the original FT corrupted with only noise, are decomposed into outer products, the weights, excluding the first weight, fall on a straight line. Further application of the inversion algorithm cannot change this because noise is uncorrelated with the FT. Noise simply cannot be described by a single outer product. The distortions that are present on the FT are a different matter. Inversion algorithms struggle to fit the distortions with a single outer product pair, resulting in a weight plot that is curved because the salient features of the FT require that multiple outer products be used to describe them. However, the distortions are correlated with the FT, which means that fewer outer products are needed for reproduction of the distortions in the FT than the number that would be required for reproduction of uncorrelated noise. That this is so is shown in the weight plots of filtered FT's 5 and 6 (Fig. 2). Although the act of filtering FT 4 removes the noise from the FT, it also distorts the FT slightly. The distortion is shown as a curve in the weight plot. Consequently, we can distinguish noise from distortions because the weights of the outer product that reproduces noise fall on nearly a straight line, whereas distortions cause a curve in the weight plot. By interpolation of a line from the noise weights at a high outer product number, noise can be separated from distortions.

Because the distortions have contributions that are spread over relatively few outer products, retrieval algorithms are more likely to fit them (FT's 5 and 6), so that they contribute relatively little to the FT error but contribute significantly to the measured pulse error. Indeed, distortion-limited convergence can be quite deleterious, producing relatively low FT errors but large errors in the reconstructed pulse (see the caption of Fig. 2).

In the next example we demonstrate the power of our technique by analyzing systematic experimental errors. Figure 5(a) shows an experimental second-harmonic-generation (SHG) FT, and Fig. 5(b) shows the retrieved pulse and gate obtained by use of the SHG-PCGP algorithm.[4,5] Because this algorithm uses a soft constraint to force the pulse and the gate to be equal, slight asymmetries between the negative and positive time delays in the SHG FT cause slightly

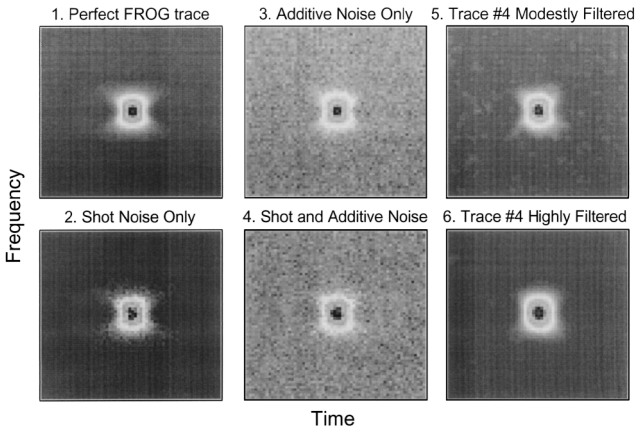

Fig. 2. Series of synthetic SHG FT's (the square root of intensity versus frequency and time delay is presented to show more detail) with cubic spectral phase and various amounts of noise and distortion: 1, perfect FT with no distortions. 2, trace with shot noise added. (It has a per-pixel rms deviation of $12V^{1/2}$, where V is the pixel value, which varies from 0 to 62,500.) 3, only additive noise added (per-pixel rms deviation of 2% of the maximum pixel value). 4, both additive and shot noise. 5, modestly filtered version of the trace 4. 6, filtered version of trace 4 but visibly distorted as a result of filtering. After pulse retrieval the FT error and the retrieved pulse error are 1, 0%, 0%; 2, 0.8%, 0.14%; 3, 2.0%, 3.5%; 4, 2.2%, 2.7%; 5, 0.44%, 3.9%; 6, 0.3%, 8.5%, respectively.

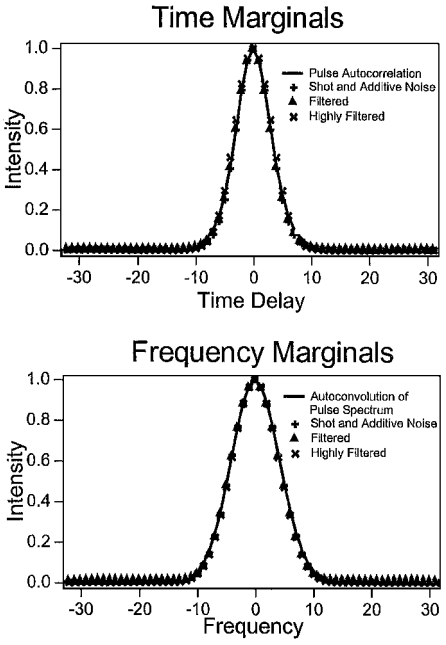

Fig. 3. Time and frequency marginals of FT's 2–4 depicted in Fig. 2. The agreement among all frequency and time marginals is excellent.

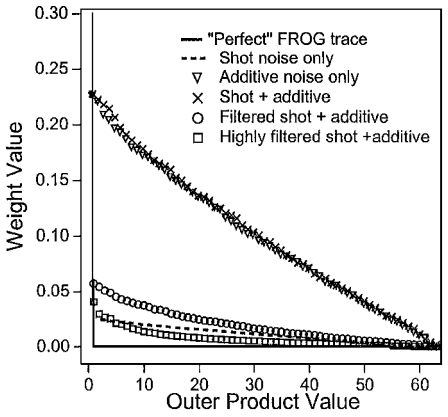

Fig. 4. SVD analysis of the FT depicted in Fig. 2. Any deviation from a straight line indicates either distortion or a lack of convergence of the algorithm. All plots are normalized to have a maximum value of 1.

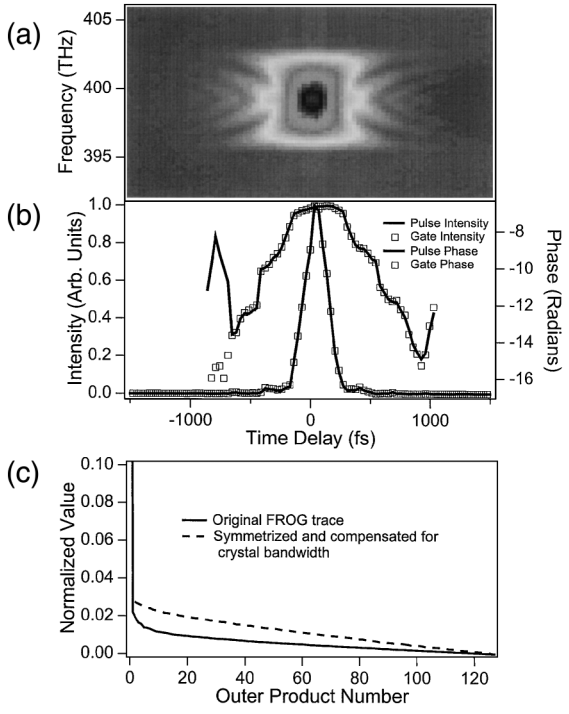

Fig. 5. (a) Experimental SHG FT (square root of the intensity). (b) Retrieved pulse. (c) SVD analysis. The SHG-PCGP algorithm was used to invert the FT. There is very little difference between the pulse and the gate, indicating that the FT is nearly symmetric. The slight curvature in the normalized weight plot indicates only a small amount of distortion. If we assume that the distortion is due only to the bandwidth limitation of the doubling crystal and compensation for it, we can achieve nearly noise-limited convergence [dashed curve in (c)].

different pulse and gate to be returned. The FT shown in Fig. 5(a) is only slightly asymmetric; as a result the differences between the retrieved pulse and the retrieved gate are minimal (0.4% difference). The weight plot from a SVD analysis shows nearly noise-limited convergence [Fig. 5(c)]. The slight curve in the weight plot is caused by FT asymmetry and some lost bandwidth that is due to group-velocity mismatch in the doubling crystal. To compensate for these distortions we average the negative and positive time delays to symmetrize the FT in Fig. 5(a) and divide the frequency axis by a Gaussian to enhance the frequency components in the wings. We apply the SHG-PCGP algorithm to the corrected FT to retrieve a new pulse. After another error analysis is completed, we can see a straight weight plot, which is indicative of noise-limited convergence [Fig. 5(c), dashed curve], and the FT error decreases from 0.4% to 0.25%. There are only negligible differences between the pulses retrieved from the original FT and from the corrected FT, so we are assured of an accurately reconstructed pulse.

This convergence analysis is quite useful; however, it is not foolproof. It is based on the principal components generalized projections algorithm, which requires the wings of the pulse intensity to approach zero. Also, any distortion that converts a FT into something that still appears to be a FT cannot be found with this method. One example is a linearly chirped SHG FT that has been amplitude limited along the time coordinate by an invalid time calibration.

In conclusion, a new, simple error analysis has been presented for testing the convergence and accuracy of FROG traces. This analysis is sensitive and general; it is algorithm independent and can be used for any spectrogram, sonogram, or FT inversion. All that is required is the retrieved pulse (and gate, if available) and the FT. This analysis separates noise and distortions, allowing one to determine whether the resulting convergence is distortion or noise limited.

D. J. Kane acknowledges the support of the National Science Foundation through grant DMI-9801116; e-mail address, djkane@swsciences.com.

References

1. D. J. Kane and R. Trebino, IEEE J. Quantum Electron. **29,** 571 (1993).
2. R. Trebino, K. W. DeLong, D. N. Fittinghoff, J. N. Sweetser, M. A. Krumbügel, B. A. Richman, and D. J. Kane, Rev. Sci. Instrum. **68,** 3277 (1997).
3. D. J. Kane, G. Rodriguez, A. J. Taylor, and T. Clement, J. Opt. Soc. Am. B **14,** 935 (1997).
4. D. J. Kane, IEEE J. Sel. Top. Quantum Electron. **4,** 278 (1998).
5. D. J. Kane, IEEE J. Quantum Electron. **35,** 421 (1999).
6. T. I. Kuznetsova and I. A. Walmsley, Quantum Electron. **28,** 728 (1998).
7. T. M. Shuman, M. E. Anderson, J. Bromage, C. Iaconis, L. Waxer, and I. A. Walmsley, Opt. Express **5,** 134 (1999); http://epubs.osa.org/opticsexpress.
8. D. T. Reid, IEEE J. Quantum Electron. **35,** 1584 (1999).
9. V. Wong and I. A. Walmsley, J. Opt. Soc. Am. B **14,** 944 (1997).
10. J. L. A. Chilla and O. E. Martinez, Opt. Lett. **16,** 39 (1991).
11. A. K. Jain, *Fundamentals of Digital Image Processing* (Prentice-Hall, Englewood Cliffs, N.J., 1989).